JOURNAL OF GEOPHYSICAL RESEARCH, VOL. 107, NO. A12, 1477, doi:10.1029/2001JA007546, 2002

Strong interplanetary magnetic field B_y-related plasma convection in the ionosphere and cusp field-aligned currents under northward interplanetary magnetic field conditions

G. Le,[1] G. Lu,[2] R. J. Strangeway,[3] and R. F. Pfaff Jr.[1]

Received 3 August 2001; revised 17 April 2002; accepted 10 September 2002; published 26 December 2002.

[1] We present in this paper an investigation of interplanetary magnetic field (IMF) B_y-related plasma convection and cusp field-aligned currents using Fast Auroral Snapshot (FAST) data and the assimilative mapping of ionospheric electrodynamics (AMIE) model during a prolonged interval with large positive IMF B_y and northward B_z conditions ($B_y/B_z \gg 1$). Using the FAST single trajectory observations to validate the global convection patterns at key times and key locations, we have demonstrated that the AMIE procedure provides a reasonably good description of plasma circulations in the ionosphere during this interval. Our results show that the plasma convection in the ionosphere is consistent with the antiparallel merging model. When the IMF has a strongly positive B_y component under northward conditions, we find that the global plasma convection forms two cells oriented nearly along the Sun-Earth line in the ionosphere. In the Northern Hemisphere, the dayside cell has clockwise convection, mainly circulating within the polar cap on open field lines. It appears to be the lobe cell convection. A second cell with counterclockwise convection is located in the nightside, circulating across the polar cap boundary. The lobe cell convection is driven by the reconnection along the antiparallel merging lines poleward of the cusp extending toward the duskside when IMF $B_y/B_z \gg 1$. The field-aligned currents in the cusp region flow downward into the ionosphere. The return field-aligned currents extend into the polar cap in the center of the dayside lobe convection cell. The field-aligned currents are closed through the Peterson currents in the ionosphere, which flow poleward from the polar cap boundary along the electric field direction. *INDEX TERMS:* 2784 Magnetospheric Physics: Solar wind/magnetosphere interactions; 2463 Ionosphere: Plasma convection; 2708 Magnetospheric Physics: Current systems (2409); *KEYWORDS:* field-aligned currents, ionosphere convection, polar cusp, northward IMF, large IMF B_y, FAST spacecraft

Citation: Le, G., G. Lu, R. J. Strangeway, and R. F. Pfaff Jr., Strong interplanetray magnetic field B_y-related plasma convection in the ionosphere and cusp field-aligned currents under northward interplanetary magnetic field conditions, *J. Geophys. Res.*, *107*(A12), 1477, doi:10.1029/2001JA007546, 2002.

1. Introduction

[2] Magnetic reconnection, originally proposed by *Dungey* [1961], is the principal mechanism in the solar wind-magnetosphere-ionosphere coupling process that transfers solar wind mass, momentum, and energy to the magnetosphere. Field-aligned currents electrically couple the outer magnetosphere to the ionosphere. They transmit the stress applied by the reconnection from the magnetopause to the ionosphere, which drives large-scale plasma convection in the magnetosphere and ionosphere.

[3] Polar cusp and cusp field-aligned currents are of great interest in the study of the coupling process since the solar wind plasma has direct access to low altitudes in this region. *Saunders* [1989] proposed a model for the origin of cusp field-aligned currents due to the dayside reconnection. In this model, the motion of newly reconnected field lines following quasi-steady reconnection at the dayside magnetopause is caused by two combined effects: the magnetic tension force on the field lines and the diverging magnetosheath flow directed radially away from the subsolar point. The newly opened field lines are pulled toward the east/west direction initially in response to the interplanetary magnetic field (IMF) B_y component, and subsequently anti-sunward in the direction of magnetosheath flow, resulting in dawnward/duskward plasma convection at field line footprints near the dayside polar cap boundary. Field-aligned currents arise where the convection flow has a vorticity that are associated with Alfven waves that transmit the stress between the magnetopause and the ionosphere [*Cowley*, 2000].

[1]Laboratory for Extraterrestrial Physics, NASA Goddard Space Flight Center, Greenbelt, Maryland, USA.
[2]High Altitude Observatory, NCAR, Boulder, Colorado, USA.
[3]Institute of Geophysics and Planetary Physics, University of California, Los Angeles, California, USA.

0148-0227/02/2001JA007546$09.00

[4] Although Saundres' model is for reconnection at the dayside magnetopause for southward IMF, the reconnection is not limited to southward IMF and occurs for other IMF orientations. As suggested in the antiparallel merging model by *Crooker* [1979], the merging between the IMF in arbitrary orientations and the Earth's magnetic field occurs preferentially at the magnetopause where the fields are antiparallel. When the IMF does not have a southward component, the merging line in the model emanates from the cusps entirely on open lobe field lines in the dusk (dawn) side in the Northern Hemisphere for positive (negative) IMF B_y component, and vice versa in the Southern Hemisphere. As a consequence, there is no flux transfer from dayside closed field lines to lobe open field lines due to the reconnection, opposite to the case for southward IMF. The polar cap convection streamlines are confined within the polar cap boundary and only transfer flux from one side of lobe to the other, the so-called lobe cell convection. For positive IMF B_y component, the antiparallel reconnection occurs in the duskside of the northern lobe, and the magnetic tension force pulls the newly reconnected field line in the Northern Hemisphere toward the dawnside. The dayside polar cap convection becomes a single vortex with streamlines from dusk to dawn in the dayside Northern Hemisphere (Figure 5 in *Crooker* [1979]).

[5] Observationally, the large-scale convection patterns in the ionosphere for northward IMF are not as well understood as those for southward IMF. Two-cell convection patterns with antisunward flow over the polar cap are consistently observed in data and predicted by models for southward IMF. However, many different convection patterns have been reported for northward IMF. *Russell* [1972] first proposed that sunward convection within the polar cap would be driven by reconnection between northward IMF and open field lines poleward of cusps. The plasma convection would form two reverse cells, a clockwise cell in the morning sector and a counterclockwise cell in the afternoon sector, circulating within the northern polar cap. *Maezawa* [1976] confirmed this prediction using ground-based magnetic field data to show observational evidence of the two reversed "lobe cells." But it was not clear in this study where the polar cap boundary was located in relation to the reversed convection cells. Later, four-cell convection patterns were reported, where two additional cells at lower latitudes with sunward flow on closed field lines in subauroral latitudes are present in addition to the two reverse cells in the polar cap [*Burke et al.*, 1979; *Reiff*, 1982; *Potemra et al.*, 1984]. Adding to the controversy are the distorted two-cell patterns reported by *Heppner and Maynard* [1987], in which the two normal cells (observed commonly for southward IMF) are distorted in a degree based on the strength of the IMF B_z as it turns northward. Although subsequent observations have shown results that agree with either the distorted two-cell patterns [*Rich et al.*, 1990; *Rich and Hairston*, 1994] or reverse two-cell/four-cell patterns [*Reiff and Heelis*, 1994; *Crowley et al.*, 1992; *Weimer*, 1995; *Ruohoniemi and Greenwald*, 1996; *Huang et al.*, 2000], it has been reported that what type of the patterns will be observed depends on the relative strength of IMF B_y and B_z components [*Knipp et al.*, 1991, 1993; *McCormac et al.*, 1991; *Lu et al.*, 1994]. The reverse two-cell/four-cell patterns occur for when IMF B_y is dominant ($|B_y|/B_z < 1$), and the distorted two-cell patterns occur when IMF B_z ($|B_y|/B_z < 1$) is dominant under northward IMF conditions.

[6] In this paper, we report observations of plasma convection in the ionosphere and cusp field-aligned currents that can be readily explained in the antiparallel reconnection framework. The observations of cusp field-aligned current and ionosphere convection were made by the Fast Auroral Snapshot (FAST) spacecraft [*Carlson et al.*, 1998] and from the assimilative mapping of ionospheric electrodynamics (AMIE) technique [*Richmond and Kamide*, 1988] during a prolonged interval when the IMF was northward and had a large positive B_y component. This interval occurred during the 14–16 May 1997 magnetic cloud event. Using the FAST single trajectory observations to validate AMIE global convection pattern at key times and key locations, we are able to obtain with great confidence the global picture of ionosphere convection dominated by lobe reconnection. In turn, it helps us to understand the morphology and source of cusp field-aligned currents.

2. IMF Observations

[7] An overview of the origins and development of the 12 May 1997 coronal mass ejection at the Sun by SOHO and subsequent interplanetary observations of the magnetic cloud at 1 AU by Wind during 14–16 May was presented in *Webb et al.* [2000]. The Wind observations of interplanetary magnetic field and solar wind plasma conditions at 1 AU were also discussed in *Jordanova et al.* [2001]. The interplanetary shock preceding the magnetic cloud was observed by Wind at 0115 UT on 15 May 2001, which was located at about 190 R_E upstream from the Earth. The shock front arrived at the Earth's magnetosphere at 01:59 UT, as seen by the Polar spacecraft (there are no FAST data available for this time). This gives a 44-min time delay from the Wind spacecraft to Earth, which is similar to the 45-min time delay estimated from average upstream solar wind speed and the lcoation of Wind. The magnetic cloud followed about 8 hours after the shock front and lasted for about 15 hours. The cloud's axial field was very strong, about 23 nT, and was nearly along the +Y direction. The helical field was left-handed, resulting in a southward followed by northward magnetic field within the cloud.

[8] Our period of interest is during the second half of the cloud, when the magnetic field was northward and had a strong positive B_y component. Figure 1 shows the IMF data in GSM coordinates during the magnetic cloud passage as observed by Wind and IMP-8 spacecraft. The labels on the horizontal axis correspond to times at Earth as the Wind data are shifted by 44 min and the IMP-8 data by 3 min to account for the lag time from the spacecraft to Earth. The bottom panel of Figure 1 shows the IMF clock angle, which is the angle of the IMF in the YZ plane. The angles of 90°, 0°, and −90° correspond to due northward, horizontal, and due southward, respectively. The four short bars are the times of successive FAST northern polar cap passes during the second half of the cloud, which we will discuss in detail in this paper. For the last three passes (orbits 2891–2893), both the IMF B_y and B_z were positive, and the IMF B_y was

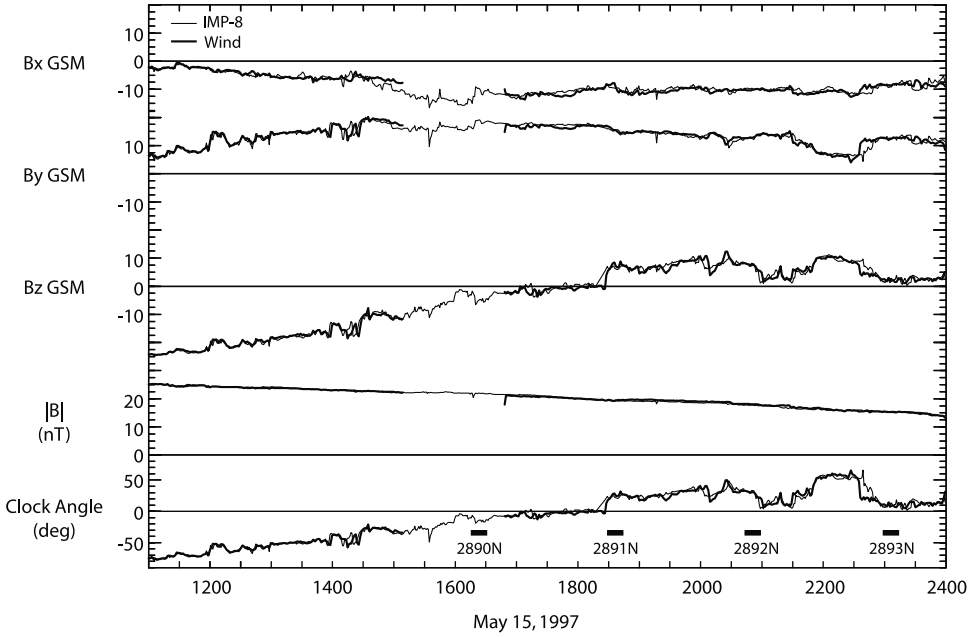

Figure 1. The interplanetary magnetic field data in GSM coordinates from Wind and IMP-8 spacecraft. The universal time corresponds to the time at Earth as the Wind data are shifted by 44 min and the IMP-8 data by 3 min to account for the lag time from the spacecraft to Earth.

the dominant component ($B_y \gg B_z$). For the first pass (orbit 2890), the IMF was slightly southward.

3. FAST Observations of Polar Cusp and Field-Aligned Currents

[9] We now present the FAST observations during polar cap passes in the Northern Hemisphere for the three northward IMF cases. During these passes, the spacecraft trajectory is near the noon-midnight meridian. The spacecraft is near its orbital perigee moving from local noon to local midnight at altitudes of ~400 to 600 km.

[10] The polar cap pass for FAST orbit 2891 occurs when the IMF just turns to slightly northward, 26° from the ecliptic plane, following more than 1 hour of nearly horizontal field. Figure 2 shows about 6 min of data near the polar cusp region, including (from top to bottom) the electron energy spectrogram averaged over all pitch angles, the electron pitch angle spectrum over the energy range from 5 to 30 keV, the ion energy spectrogram averaged over all pitch angles, the ion pitch angle spectrum over the energy range from 40 to 30 keV, the density of field-aligned currents, and the residuals of the magnetic field component from IGRF 95 model field in local field-aligned coordinates. The labels in the bottom of Figure 2 include the universal time, spacecraft altitude in kilometers, as well as the magnetic latitude and local time of the spacecraft footprints in the ionosphere.

[11] The plasma data in top four panels in Figure 2 are from the ion and electron electrostatic analyzers on FAST. In the Northern Hemisphere, 0° pitch angle corresponds to downgoing, field-aligned particles, and 180° pitch angle corresponds to upgoing plasma. The polar cusp is characterized by the localized, intense field-aligned particle precipitations. Equatorward of the cusp particle precipitations, the spacecraft is on closed field lines of the dayside magnetosphere, as evidenced by the presence of trapped high-energy (~1–10 keV) electrons, low energy (~10 eV) photoelectrons escaping from the ionosphere, and double loss cones of ions at 0° and 180° pitch angles in the beginning of the interval. The disappearance of high-energy trapped electrons occurs at the equatorward boundary of cusp precipitations. Apparently this is the dayside polar cap boundary, i.e., the boundary between open and closed field lines.

[12] Poleward of the polar cap boundary, intense ion and electron precipitations are observed in a localized cusp region spanning 4.8° in magnetic latitude (from 73.3° at 1832:55 UT to 78.1° at 1834:05 UT) at 1245 magnetic local time (MLT) at spacecraft footprints. The flux of cusp ions centers at 1 keV but has a broad energy range from ~0.1 to 10 keV. Within the same region, the bulk of the electrons occurs within a narrow energy band centered at a few hundred electron volts, and the maximum energy only reaches ~1 keV. These cusp precipitations are mainly of magnetosheath origin.

[13] As the spacecraft moves away from the cusp region to the polar cap, the ion precipitation is nearly absent, but there are electron precipitations with energy of the order of kiloelectron volts extending to high latitudes. These electrons appear to be inverted-V precipitations produced by an upward-directed parallel electric field [e.g., *Block and Falthammar*, 1990]. At the spacecraft altitude of ~400 km in this pass we do not observe upgoing lower-energy (few hundred electron volts) ion beams and ion conics that are also associated with an upward-directed parallel electric field, such as those observed at ~4000 km altitude by FAST [*Pfaff et al.*, 1998]. Thus, the local acceleration region with parallel electric field is above the spacecraft altitude of ~400 km in this pass. We can treat the magnetic field lines from spacecraft to the ionosphere below as equal-potential lines as we map the in situ observations to the ionosphere later.

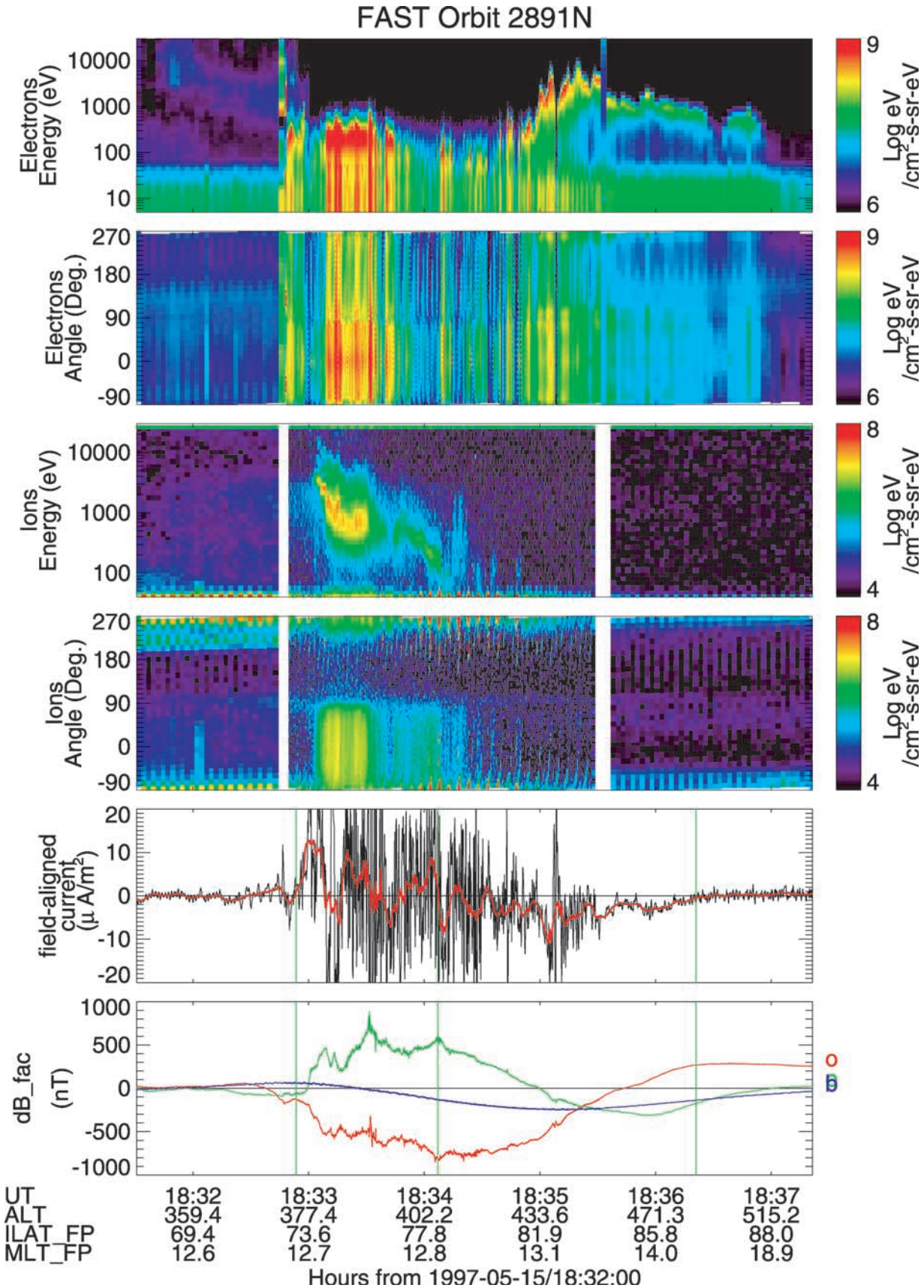
FAST Orbit 2891N
Electrons Energy (eV)
10000
1000
100
10
9
6
Log eV /cm²-s-sr-eV
Electrons Angle (Deg.)
270
180
90
0
-90
Ions Energy (eV)
8
4
Ions Angle (Deg.)
field-aligned current (μ A/m²)
20
10
0
-10
-20
dB_fac (nT)
1000
500
-500
-1000
O
B
UT 18:32 18:33 18:34 18:35 18:36 18:37
ALT 359.4 377.4 402.2 433.6 471.3 515.2
ILAT_FP 69.4 73.6 77.8 81.9 85.8 88.0
MLT_FP 12.6 12.7 12.8 13.1 14.0 18.9
Hours from 1997-05-15/18:32:00

[14] In the bottom panels of Figure 2 are the magnetic field observations and deduced field-aligned current density. The local field-aligned coordinate system is defined such that **b** (blue trace) is field-aligned direction, **e** (green trace) points eastward and is the cross product of **b** and radial direction **r**, **o** (red trace) is outward, and **o**-**e**-**b** forms a right-handed system. The density of field-aligned currents is calculated based on the magnetic field perturbation by assuming that they are infinite sheet currents locally normal to the magnetic meridian plane. As we will demonstrate using simultaneous observations of magnetic field and electric field, this appears to be a valid assumption. The current density j at the spacecraft altitude is the differentiation of the magnetic field cross-track component δB (which is mainly the east-west component δB_e) with respect to the distance along the spacecraft cross-field track x, or $j = (1/\mu_o) \cdot \{\partial(\delta B)/\partial x\}$. The red trace is spin-average smoothed current density. The positive sign of j is for current flowing downward into the ionosphere and the negative for current upward, away from the ionosphere.

[15] Despite embedded fine-structure currents, the overall field-aligned currents consist of a pair of large-scale currents with opposite polarity (bracketed by vertical lines) from the magnetic field and the current density profiles: a downward current corresponding to positive slope in the east-west component of the magnetic field and an upward current corresponding to negative slope in the east-west component of the magnetic field as the spacecraft moves to higher latitudes. Both the large-scale current sheets are on open field lines, poleward of the polar cap boundary. It is apparent that the downward current is coincident with the particle-entry cusp. The upward current extends to the polar cap within the region of inverted-V electron precipitations.

[16] The subsequent two passes of the polar cap (orbits 2892 and 2893) during the interval of interest show similar features of the cusp and field-aligned currents. Figure 3 displayed about 7 min of data near the Northern Hemisphere polar cusp region for FAST orbit 2892 in the same format as Figure 2. During this pass, the average IMF has a clock angle of 30° from the ecliptic plane. The polar cap boundary is observed at 74.3° invariant latitude at the spacecraft footprint. The polar cusp, characterized by intense precipitations of both ions and electrons, occurs from ~2047:16 to 2048:12 UT, spanning ~3.8° in invariant latitude at ~1138 MLT. Poleward of the polar cusp and inside the polar cap, we again see inverted-V electron precipitations. From the magnetic field data and deduced current density, it is clear that the cusp field-aligned currents consist of a pair of current sheets: the downward flowing current sheet is coincident with the particle entry cusp (74.3° to 78.1° ILAT), and the upward flowing current sheet extends into the region with inverted-V electron precipitations in the polar cap (above 78.1° ILAT), similar to what we see in the previous pass.

[17] Figure 4 shows about 4 min of data near the polar cusp region in the Northern Hemisphere for FAST orbit 2893 in the same format as Figure 2. During this pass, the IMF has an average clock angle of 11° from the ecliptic plane. The polar cap boundary is observed at 76.9° ILAT at the spacecraft footprint. The particle entry cusp with intense precipitations of both ions and electrons occurs from ~2302:29 to 2303:25 UT, spanning ~5.0° in invariant latitude at ~1059 MLT. Poleward of the cusp region and inside the polar cap, the inverted-V electron precipitations are present. Again, a pair opposite-directed large-scale field-aligned currents are observed, but the current density is smaller than in the previous two passes. In this pass, the downward flowing current is coincident with the most intensive particle precipitations in the equatorward portion of the particle entry cusp, from ~76.9° to 80.4° ILAT (2302:29 to 2303:25 UT) at ~1107 MLT. The upward flowing current overlaps with the poleward edge of the particle entry cusp and extends well into the polar cap, with inverted-V electron precipitation (above 80.4° ILAT).

[18] We examine next the simultaneous observations of the magnetic field and electric field in the field-aligned current region for the three passes. Figure 5 shows the east-west component of magnetic field δB_e (red traces) and the electric field component in the spacecraft spin plane (blue traces). The electric field component is labeled *E_ALONG_V* because the spacecraft spin axis is nearly perpendicular to the spacecraft orbit plane and the spacecraft velocity $\boldsymbol{V}_{s/c}$ thus lies nearly in the spin plane. It is mainly in the north-south direction for these passes. The values of *E_ALONG_V* shown here are obtained by spin fits to the high-resolution data and are available every half spin (~2.5 s). The motional electric field, $\boldsymbol{V}_{s/c} \times \boldsymbol{B}$, although very small in the spin plane, has been removed.

[19] In Figure 5, it is evident that there is a very good correlation between the two independently measured quantities in the paired field-aligned current region. The large-scale structures of both quantities track each other very well in the field-aligned current region. A linear correction between the east-west magnetic field and the north-south electric field is a consequence in a model where field-aligned currents are approximately to be infinite two-dimensional sheets and the current closure circuit is mainly in the meridian plane via Pederson currents [*Smiddy et al.*, 1980]. Significant divergence via Hall currents in the east-west direction will result in a poor correlation between the two quantities [*Sugiura et al.*, 1982].

4. Plasma Convection in the Ionosphere

[20] We present in this section plasma convection patterns in the polar ionosphere during the period of interest derived from the AMIE technique. The plasma convection in the ionosphere is driven by the solar wind-magnetosphere-ionosphere coupling via field-aligned currents. Thus the convection pattern along with the knowledge of ionospheric conductivities contains a wealth of information on the

Figure 2. (opposite) FAST data near the polar cusp region for orbit 2891 including (from top to bottom) the electron energy spectrogram averaged over all pitch angles, the electron pitch angle spectrum over the energy range from 5 to 30 keV, the ion energy spectrogram averaged over all pitch angles, the ion pitch angle spectrum over the energy range from 40 eV to 30 keV, the density of field-aligned currents, and the residuals of the magnetic field component from the IGRF 95 model field in local field-aligned coordinates.

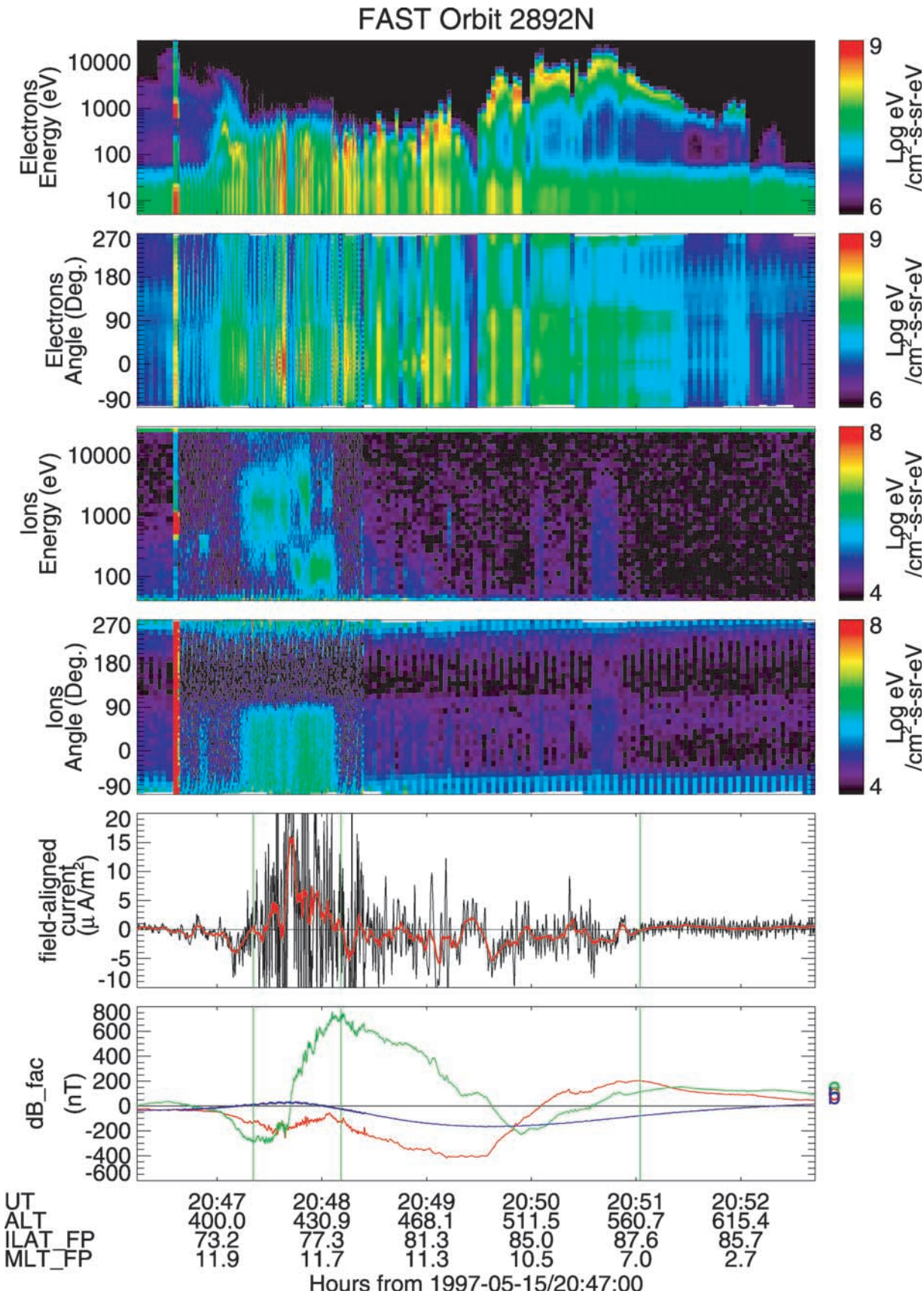

Figure 3. FAST data from near the polar cusp region for orbit 2892 in the same format as in Figure 2.

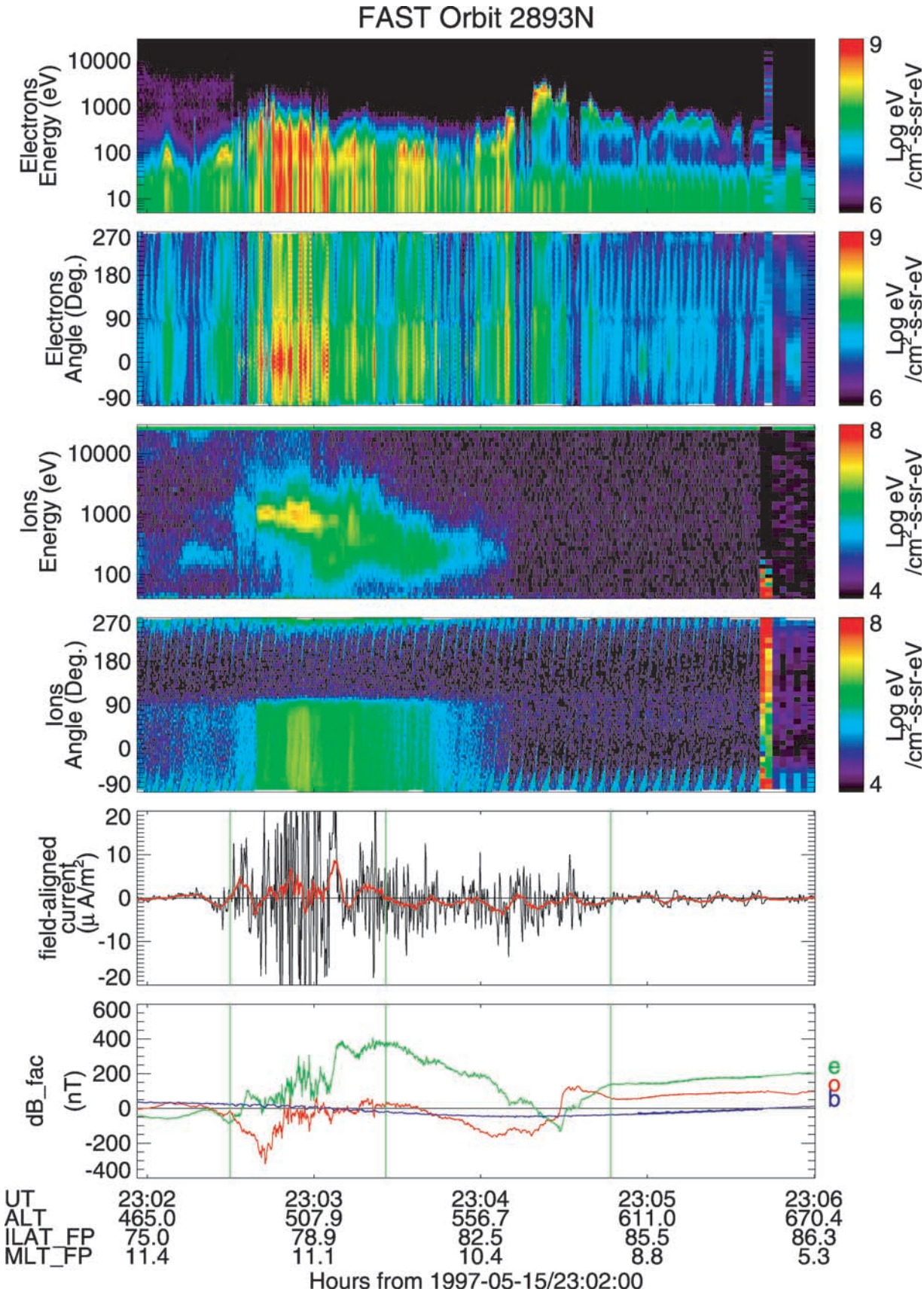

Figure 4. FAST data from near polar cusp region for orbit 2893 in the same format as in Figure 2.

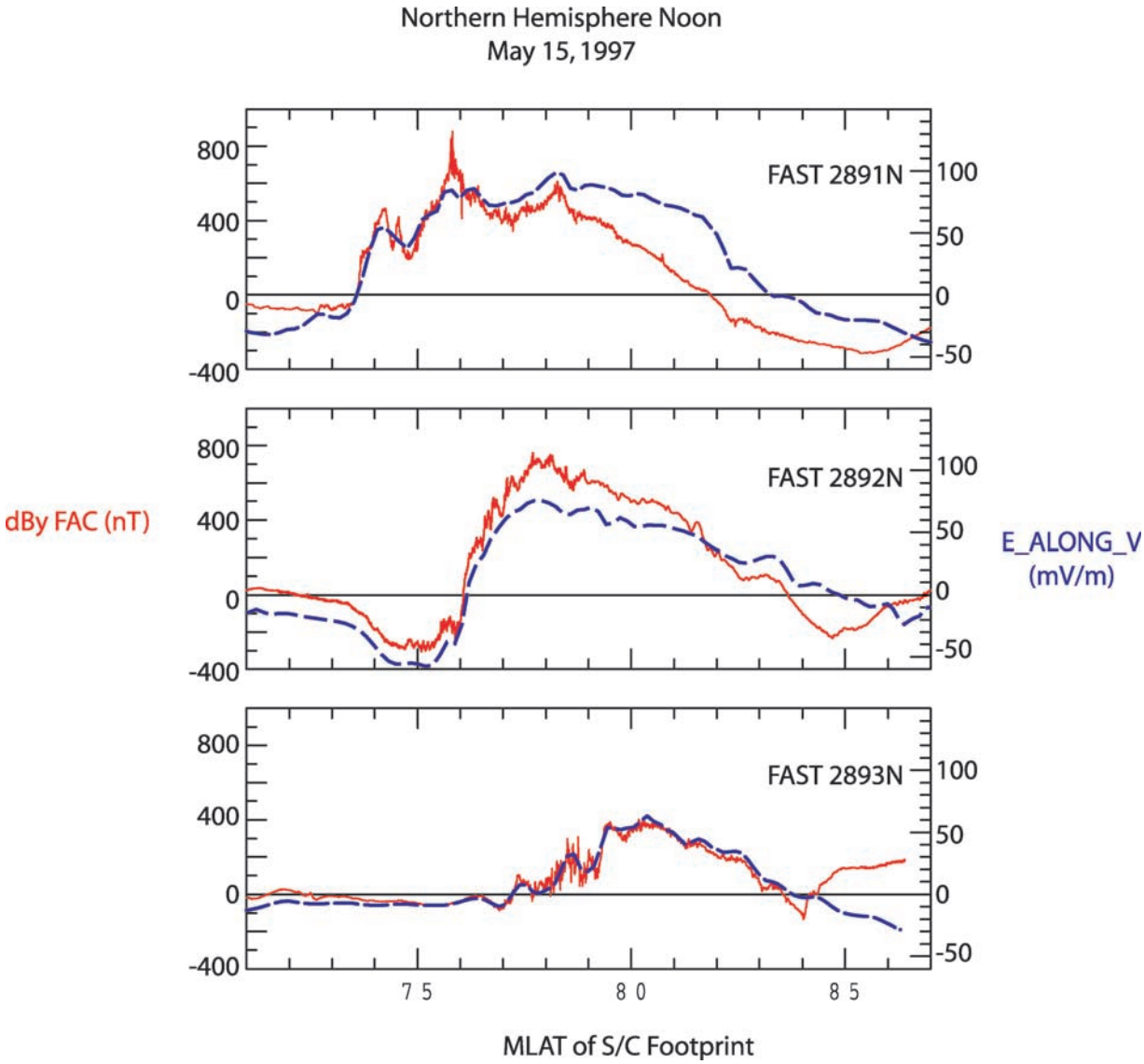

Figure 5. FAST magnetic and electric field data in the field-aligned current region. The red and blue traces are the east-west component of magnetic field, δB_e, and the electric field component in the spacecraft spin plane, respectively.

global morphology and distribution of the field-aligned currents. The AMIE technique provides snapshots of global ionospheric convection patterns by combining simultaneous global ground-based and space-based observations. From FAST magnetic field and electric field data we can obtain the plasma cross-track convection velocity along the spacecraft pass. With FAST observations to validate the AMIE global picture at key times and key locations, we can obtain with great confidence the information on the source and spatial extent of the field-aligned currents.

[21] In Figures 6, 7, and 8, we compare simultaneous AMIE convection patterns and field-aligned current distributions with FAST observations along the spacecraft orbits presented in the previous section. The AMIE patterns are derived based on a 12-min window of radar and satellite observations centered at key times of FAST cusp crossings (1835 UT for orbit 2891, 2050 UT for orbit 2892, 2305 UT for orbit 2893). The left panels show the AMIE convection patterns, where the dashed contours represent negative electric potentials, or clockwise plasma convection, and the solid contours represent positive potentials, or counter-clockwise plasma convection, with a contour interval of 5 kV. The plus and minus signs indicate the locations with most positive and negative potentials, respectively. The right panels show corresponding field-aligned currents distribution at the key times, where the solid contours are for currents flowing downward into the ionosphere and the dashed contours are for currents flowing upward, away from the ionosphere.

[22] The FAST observations are overlain on the AMIE patterns along the track of spacecraft footprints in Figures 6, 7, and 8. The blue arc segments mark the polar cap boundary identified based on FAST plasma data. The blue dots along the spacecraft footprints give 5-min tick marks, and the blue line marks the terminator at the field line footprints. In the left panels, the red vectors along the track are the equivalent $\boldsymbol{E} \times \boldsymbol{B}$ flow velocities at the spacecraft

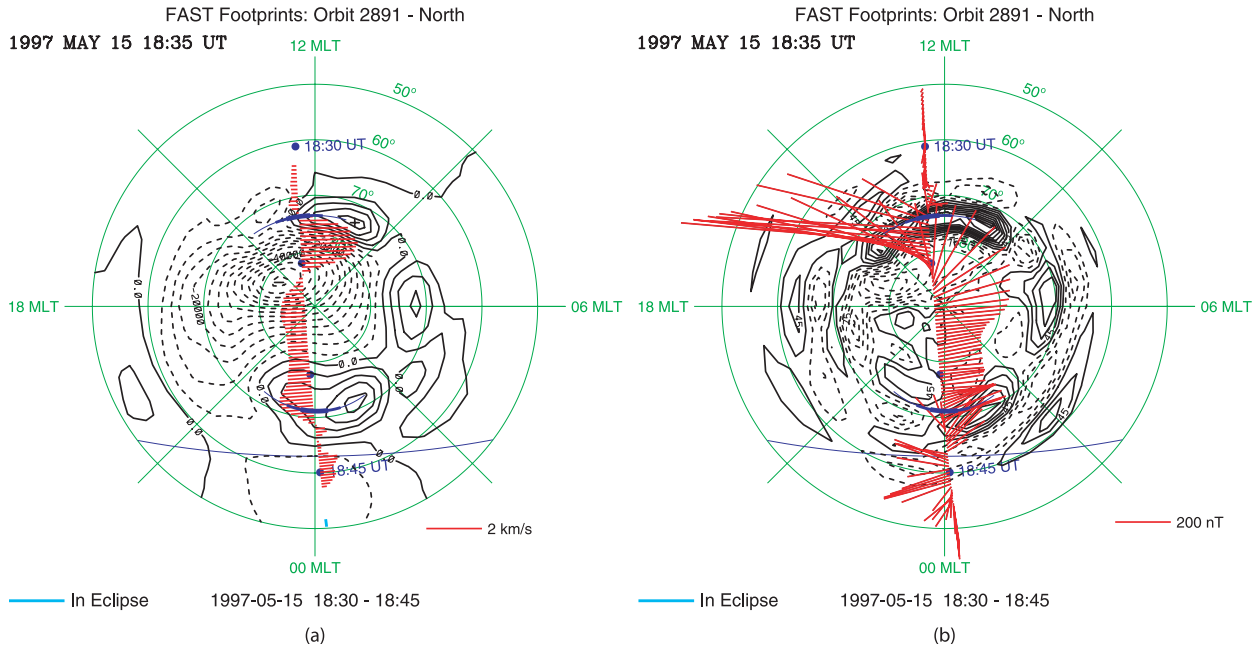

Figure 6. The FAST observations are overlain on the AMIE patterns along the track of spacecraft footprints for orbit 2891: (a) The FAST observation of the plasma convection velocity and the AMIE convection pattern. (b) The FAST observation of the magnetic field perturbation and the AMIE field-aligned current distribution pattern. The IMF was northward with a large positive B_y component during this interval.

plotted along the spacecraft ionosphere footprints. In the right panels, the red vectors are the polar projections of the transverse magnetic field perturbations along the track of spacecraft footprints. In the calculation of the plasma convection velocity at FAST, the transverse magnetic field perturbations include both the along-track and cross-track components, but the electric field data only includes the along-track component (*E_ALONG_V*), and thus, the convection flow velocity is only determined for the nearly cross-track component. Nevertheless, the cross-track flow

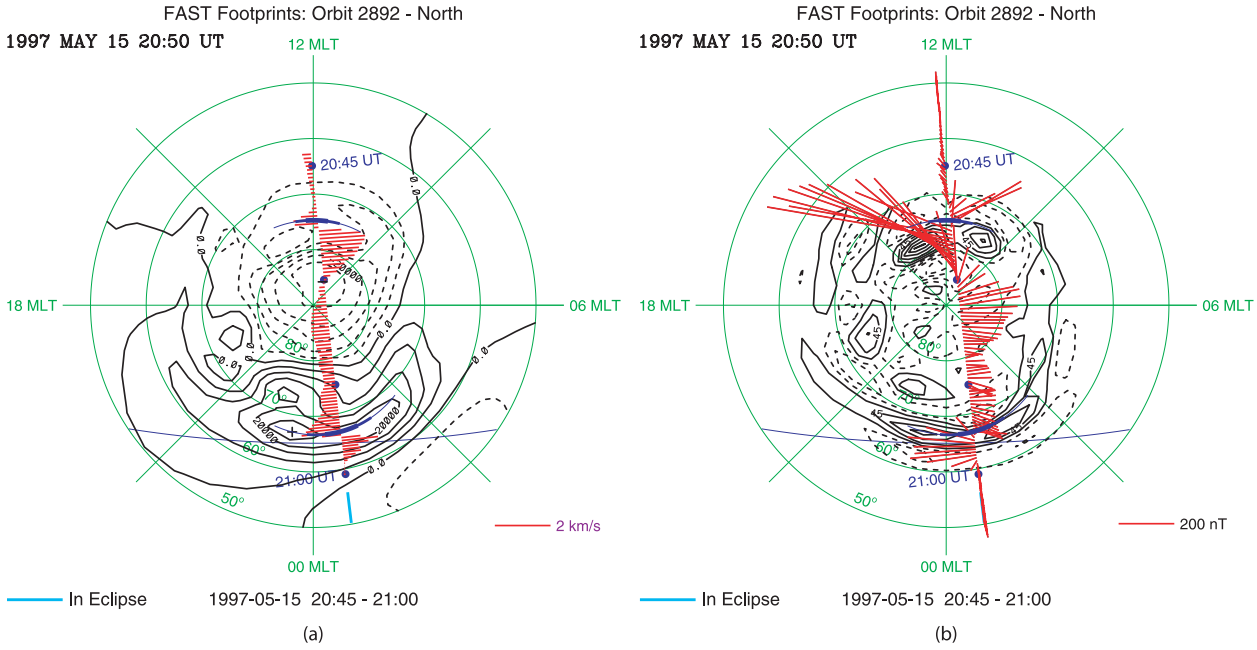

Figure 7. The FAST observations are overlain on the AMIE patterns along the track of spacecraft footprints for orbit 2892 in the same format as in Figure 6. The IMF was northward with a large positive B_y component during this interval.

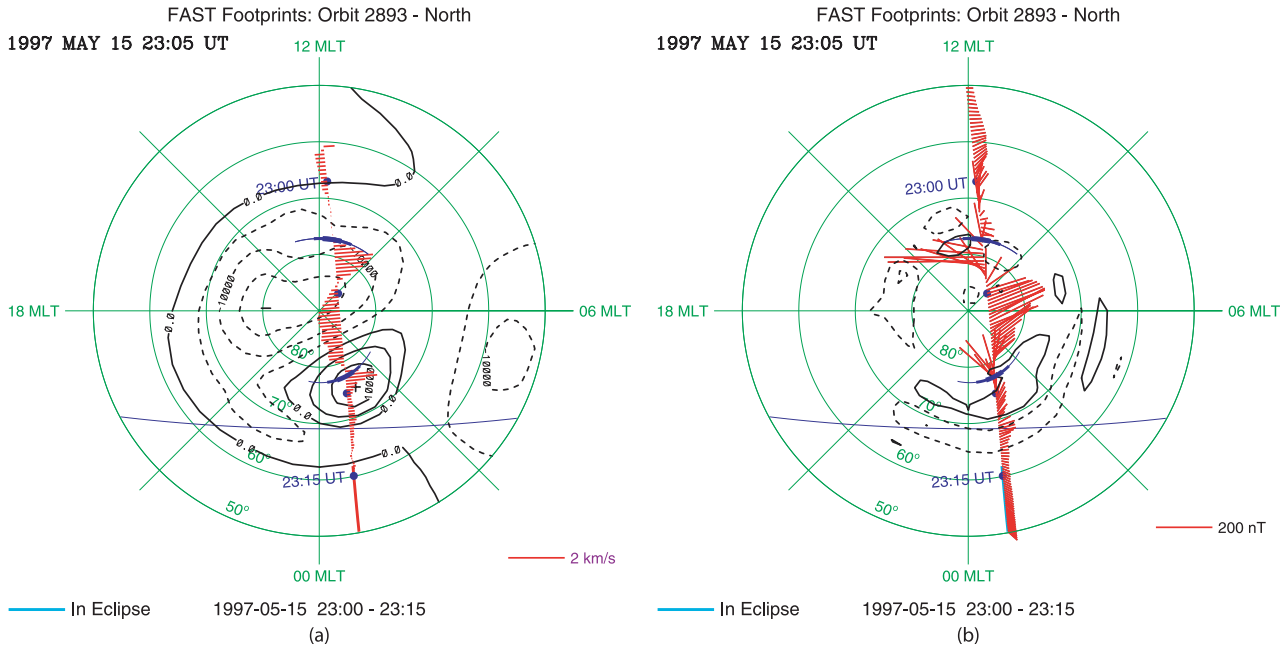

Figure 8. The FAST observations are overlain on the AMIE patterns along the tack of spacecraft footprints for orbit 2893 in the same format as in Figure 7. The IMF was northward with a large positive B_y component during this interval.

velocity appears to be the dominant component along the FAST trajectory when compared with the AMIE convection patterns. In Figures 6, 7, and 8, it is remarkable that the equivalent flow velocity along the track of FAST footprints is in excellent agreement with the main features in the large-scale AMIE convection patterns near the polar cusp region (which corresponds to the key times the AMIE snapshots are taken). The direction of the flow velocity and the flow reversal sites at FAST match the AMIE convection pattern very well during the key time intervals.

[23] In the left panel of Figure 6 (1835 UT for FAST orbit 2891), the total potential difference between the locations with plus and minus signs is 90 kV. The large-scale convection pattern is dominated by a negative potential, clockwise convection cell, which has ~65 kV in potential difference. The dominant cell is centered near 82° magnetic latitude in the postnoon sector. The plasma circulation in the dominant cell is mainly confined to the polar cap. The positive potential region contains more structured convection cells, with ~25 kV of potential difference, and is confined in a crescent-shaped region in the morning sector.

[24] From the AMIE pattern of field-aligned currents distribution (the right panel of Figure 6), it is apparent that the major current systems are located in the cusp region and the dayside polar cap. The currents with the largest density, namely the cusp currents, are flowing downward into the ionosphere, just as seen by FAST. The location of maximum current density is poleward of the FAST polar cap boundary at the dayside edge of the dominant convection cell, where the plasma convection is from dusk to dawn. The longitudinal extent of the cusp currents is about 7 hours, from 0900 to 1600 MLT and centers slightly after local noon. The upward return currents are found mainly poleward of the cusp currents and extend to most of the dayside polar cap. The maximum current density for the return currents occurs near the center of the dominant convection cell.

[25] In the next snapshot of AMIE convection pattern for FAST orbit 2892 (the left panel of Figure 7), we see a reduced overall convection level. The total potential difference decreases to 59 keV. The large-scale convection evolves into a two-cell pattern with two nearly balanced cells oriented nearly along the sun-earth line. The sunward cell is with negative potential and clockwise convection, and the antisunward cell is with positive potential and anticlockwise convection. In the right panel of Figure 7, the field-aligned currents in the dayside show similar distribution pattern: downward cusp currents located poleward of the polar cap boundary and upward return currents extending into the polar cap. Again, the mapping between the field-aligned currents and plasma convection pattern is similar to the previous pass: the downward cusp currents are located at the dayside edge of the clockwise convection cell where the plasma moves from dusk to dawn, and the upward return currents center at the center of the convection cell.

[26] In the convection pattern for FAST orbit 2893 (the left panel of Figure 8), overall convection level is further reduced. The total potential difference decreases to 31 kV. Nevertheless, the convection pattern continues to show two cells oriented nearly along the Sun-Earth line. In the right panel of Figure 8, the field-aligned currents become much weaker compared with the previous two cases. In the dayside, the downward currents in AMIE pattern are confined in a very small region in the postnoon sector (~12 to 14 MLT) poleward of polar cap boundary, and the upward currents are all over the rest of the polar cap. The weakening of the plasma convection and field-aligned currents is also evident in the FAST data. FAST observations of weak downward currents poleward of the polar cap boundary in

the cusp region and upward return currents in the polar cap (Figure 4) agree with the AMIE model. However, the longitudinal extent of the downward cusp currents in AMIE pattern does not match the FAST observation precisely. In the FAST data, the downward cusp currents are present poleward of the polar cap boundary at least 1 hour from local noon in the prenoon sector.

[27] To understand the evolution of the convection patterns during this interval, it is helpful to show the convection pattern at 1620 UT key time for FAST orbit 2890, when the IMF was weakly southward with strong positive B_y component prior to the extended northern IMF interval (see Figure 1). Figure 9 shows a snapshot of the AMIE convection pattern as well as FAST data for FAST orbit 2890 at dayside key time. Again, the plasma convection observed along the FAST track agrees very well with the AMIE pattern in the dayside. The AMIE convection pattern shows rather familiar merging cells for positive IMF B_y and southward B_z, where a round clockwise convection cell with negative potential is on the duskside and a crescent counterclockwise convection cell with positive potential on dawnside [e.g., *Heelis*, 1985; *Crooker and Rich*, 1993; *Cowley*, 2000]. The centers of both cells are near the polar cap boundary inferred from the FAST data; thus, the magnetic flux is being transferred continuously between the open field lines and closed field lines. This is a clear indication that the reconnection site is on closed field lines equatorward of the cusp even when the IMF is slightly southward, with a large B_y component.

[28] In comparison with the convection pattern in Figure 6a, we still see some plasma convection across the polar cap boundary but with much weaker strength, which appear to be the residuals of the decaying merging cells from the previous southward IMF interval. The merging cells continue to decay and eventually reduce to a single cell in the midnight sector, as evident in Figures 7a and 8a. The major difference is the existence of a new clockwise convection cell that is mainly confined within the dayside polar cap when IMF turned northward. The plasma convection within the dayside polar cap does not involve a net transfer of magnetic flux between the open and closed field line regions and thus is driven by the reconnection between the IMF and the open field lines poleward of the cusp, as described in *Crooker* [1979, 1988]. For the cases with a very large positive IMF B_y component, the antiparallel reconnection site moves to duskside of the northern lobe. The newly reconnected field moves mainly from duskside to dawnside due to the field tension, which drives the dusk-to-dawn plasma convection in the cusp region of the ionosphere, just poleward of the polar cap boundary. The reconnected field lines will then be swept tailward, resulting in a single clockwise convection cell in the dayside northern polar cap.

[29] Having understood the plasma convection in this reconnection-driven scenario, the observed morphology of cusp field-aligned currents fits in readily. The dayside clockwise convection cell has negative potential, and the electric field points northward (or poleward), from the polar cap boundary to the center of the convection cell, in the cusp region. The field-aligned currents in the cusp region flow downward into the ionosphere, where there are velocity shears at the dayside boundary of the convection cell. They feed into the closure Peterson currents that flow poleward in the direction of electric field. Then the Peterson currents feed into the return field-aligned currents in the center of the convection vortex, which flow upward out of the ionosphere. The data also imply that the closure of the field-aligned currents mainly through the Peterson currents (Figure 5), and thus, the Hall currents close wholly within the ionosphere. This is also consistent with the fact that the cusp and the polar cap are fully illuminated by sunlight so that ionospheric conductivities are nearly uniform.

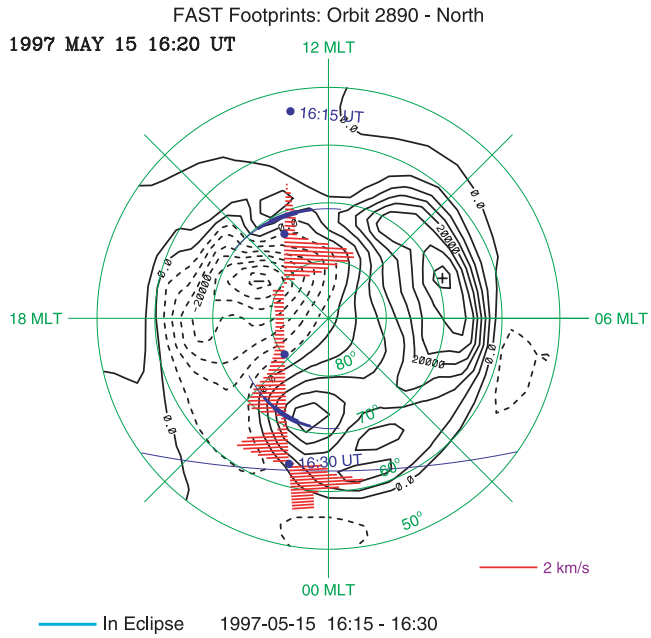

Figure 9. The FAST observation of the plasma convection velocity is overlain on the AMIE convection pattern along the track of spacecraft footprints for orbit 2890. The IMF was slightly southward with a large positive B_y component during this interval.

5. Discussion

[30] In this study, the large-scale convection patterns observed for strongly positive IMF B_y and northward B_z ($B_y/B_z \gg 1$) conditions exhibit two cells oriented nearly along the Sun-Earth line. The sunward (antisunward) cell has negative (positive) potential with clockwise (counterclockwise) plasma circulation. The observed instantaneous convection patterns differ in various degrees from statistically derived convection patterns. Although the sense of the plasma convection appears to be similar to that in the distorted two-cell statistical model for weakly northward IMF [*Heppner and Maynard*, 1987], the observed patterns in this study appear to be different in origin. In the distorted two-cell model, the normal convection cells for southward IMF were twisted and rotated to fit the observed plasma convection for northward IMF, though *Heppner and Maynard* [1987] did not offer an explanation of the underlying physical mechanisms. For the positive IMF B_y condition, the afternoon clockwise convection cell was distorted into the morning cell area to form the distorted two-cell pattern. However, the convection for southward IMF transfers magnetic flux between open and closed field line regions,

and the normal convection cells center at the polar cap boundary. It is not discussed how the convection configuration changes related to the open-closed field line boundary during the distortion of the normal cells in *Heppner and Maynard* [1987]. In this study, the dayside convection cell is observed to be mainly circulating within the polar cap on open field lines. It appears to be a new cell that is developed after the IMF turns northward, rather than a distorted afternoon cell from the southward IMF period. The decay of the two normal cells when the IMF turned from southward to northward is apparent in the evolution of the convection cells.

[31] The observed convection patterns in this study are consistent with those driven by reconnection poleward of cusps. They are similar to the reverse two-cell/four-cell statistical patterns with respect to their driving mechanisms but still differ in details. Recent statistical convection patterns derived either from spacecraft observations [*Weimer*, 1995] or from ground-based high-frequency radar observations [*Ruohoniemi and Greenwald*, 1996] clearly showed two additional convection cells developed at high latitudes to form the four-cell pattern when the IMF rotated from southward to strongly northward ($B_z > |B_y|$). The two additional cells are lobe cells with reverse convection. One of the lobe cells in the polar cap will grow at the expense of the other one as the strength of the IMF B_y increases. For positive IMF B_y, the negative potential cell in the morning will grow at the expense of positive potential cell in the afternoon. Under extreme conditions with strong positive B_y, the four-cell patterns may turn into the three-cell patterns, where there exists only a single negative potential lobe cell within the polar cap, and the viscous-like cells at the lower latitudes remain the same. The negative potential viscous-like cell at dusk and the negative potential lobe cell within the polar cap may combine into a larger negative potential cell in the afternoon sector, so that the convection pattern may appear to be unbalanced two cells nearly along the dusk-dawn meridian for strong positive B_y [*Weimer*, 1995]. But the two cells seen in this study are oriented nearly along the Sun-Earth line. This is a feature that does not appear in ''average'' patterns from statistical studies.

[32] The dayside cell in this study has the same characteristics as the expanded morning lobe cell in the reverse two-cell patterns. It can be identified as the single lobe cell confined within the polar cap driven by the reconnection poleward of the cusp under strongly positive IMF B_y conditions [*Crooker*, 1992; *Crooker and Rich*, 1993; *Hill*, 1994]. However, we see an additional cell in the nightside circulating across the polar cap boundary. This cell does not appear to be the viscous-like cell in the four-cell or unbalanced two cell patterns. Numerous models and observations have shown asymmetries of the dawn and dusk cells about the noon-midnight meridian, which is controlled by the IMF B_y component [*Burch et al.*, 1985; *Troshichev*, 1990; *Knipp et al.*, 1993; *Lu et al.*, 1994; *Burke et al.*, 1994]. The viscous-like cell appeared to be a crescent-shaped cell in the dawnside of the Northern Hemisphere for positive IMF B_y. We are not aware of any observational reports of viscous-like cells located in the nightside of the lobe cell.

[33] Recent global magnetohydrodynamics (MHD) simulation studies of the coupled magnetosphere-ionosphere convection under northward IMF B_z and large IMF B_y conditions reveal insights in mapping the ionospheric convection into the magnetosphere and suggest that both the dayside and nightside cells are driven by the reconnection [*Crooker et al.*, 1998; *Fedder et al.*, 1998; *Tanaka*, 1999; *Raeder et al.*, 2000]. All these simulations have reinforced the existence of the lobe cell convection circulating on open field lines driven by reconnection between the open lobe field lines and the IMF. The lobe cell appears as a round-shaped cell, with the sense of circulation depending on the sign of the IMF B_y component, clockwise for positive IMF B_y and counterclockwise for negative IMF B_y in the Northern Hemisphere. Along one ionospheric convection streamline (or equipotential contour) in the lobe cell, the magnetic field lines are all open, with one end connected to the ionosphere and the other end in the solar wind. These field lines map to the surface of the magnetosphere down the tail [*Tanaka*, 1999]. For positive IMF B_y, the field lines with footprints in the duskside are convected sunward in the ionospheric footprints but antisunward in their solar wind ends. They have kinks on the earthward side and appear to be newly reconnected field lines (Figure 4 of *Crooker et al.* [1998], Plate 1 of *Tanaka* [1999], Figure 5 of *Raeder et al.* [2000]). The motion of their ionospheric footprints are decoupled from the motion of their solar wind ends because these field lines are connected to the reconnection site at the high latitude magnetopause, a diffusion region with parallel potential drop along the field lines [*Crooker et al.*, 1998]. To complete one full cycle of circulation, these field lines are subsequently convected dawnward and antisunward at the footprints as they are pulled by solar wind flow and the magnetic tension force. When their footprints are in the dawnside of the convection streamline, the field lines are convected antisunward at both the ionospheric footprints and the solar wind ends. The magnetospheric ends of the field lines then enter the tail lobe from the dawn flank and drift near the surface of the northern lobe toward the dusk flank. Their shapes appear as regular open lobe field lines before they reconnect again with the IMF.

[34] The MHD simulations also show how the reconnection generates merging cells in addition to the lobe cell discussed above. These simulations suggest similar global convections in driving these merging cells, although their locations are slightly different, probably due to different solar wind conditions used in the simulations. In *Crooker et al.* [1998], the merging cells appear as a large, round-shaped cell surrounding the lobe cell in the duskside and a crescent-shaped cell in the dawnside for positive IMF B_y in the Northern Hemisphere. The round merging cell is driven by dayside reconnection between the IMF and closed magnetospheric field lines in the Northern Hemisphere. The full circulation is completed by a subsequent reconnection of open tail lobe field line and closed magnetospheric field line in the Northern Hemisphere with the location of the merging site at the dusk flank of the magnetosphere rather than in the middle of the tail. The dawnside crescent merging cell is driven by reconnection between the IMF and closed magnetospheric field lines in the Southern Hemisphere. In the simulation of *Tanaka* [1999], the merging cells are driven by a similar mechanism, but the crescent cell would be located in the nightside premidnight for negative IMF B_y and postmidnight sector for positive IMF B_y. In Figure 6 of *Tanaka* [1999] (for negative IMF B_y), the magnetic field

lines mapped to a streaming line of the nightside merging cell clearly show sharp kinks on open field lines at the southern dusk flank of the magnetosphere. The simulation shows that the kinks are caused by recent reconnection between the earlier open lobe field lines (that are opened by earlier dayside reconnection between the IMF and the dayside closed field line) and the nightside closed field line near this site. These new open lobe field lines are convected into the lobe and become the lobe field lines nearest the dusk plasma sheet. Subsequently they go through another reconnection near the dusk plasma sheet to become close again to complete a full circulation along the premidnight clockwise crescent cell. The overall two-cell pattern is oriented more aligned to the noon-midnight meridian in *Tanaka* [1999] than in *Crooker et al.* [1998].

[35] The global MHD simulation by *Raeder et al.* [2000] during an interval of stable northward IMF B_z and negative IMF B_y shows convection patterns that closely resemble those observed in this study, with two cells oriented nearly along the Sun-Earth line (Figure 7 of *Raeder et al.* [2000]). Note that their Figure 7 should be flipped about the noon-midnight meridian and sign of the potential in each cell should be reversed for comparison with the results in this study for positive IMF B_y. In this simulation, the dayside cell is situated over the magnetic pole as lobe cell convection. It is driven by the reconnection between the open lobe field lines and the IMF occurring in a region of limited spatial extent near the dawn terminator where the IMF is antiparallel to the lobe. The location and the size of the reconnection site are very stable in the simulation under steady IMF conditions. When mapping the dayside lobe cell to the magnetotail, the tail convection pattern shows that the newly reconnected field lines drape over the dayside magnetosphere from dawn to dusk, enter the north lobe at a high latitude duskward "appendix," and then are slowly convected back across the lobe toward dawn to replace the magnetic flux stripped away from the tail by the reconnection.

[36] Mapping of the nightside cell to the magnetotail reveals a singular plasma entry point in the tail. In the simulation of *Raeder et al.* [2000], the long stretch of the nightside polar cap boundary (open-closed field line boundary) cuts through the nightside cell maps to essentially one singular point in the tail, which is the southern tip of dusk "appendix" of the northern lobe. Since ionospheric flow streamlines cross the polar cap boundary in the nightside cell, the corresponding tail flow streamlines form a strong bunching at the singular point. It is the primary "entry window" that allows solar wind plasma and magnetic flux to enter the magnetotail, and it is located almost opposite to the dawn IMF-lobe reconnection site for negative IMF B_y. This is in agreement with the reconnection site being at the dusk plasma sheet when the open lobe field lines become close along the premidnight crescent cell for negative IMF B_y in *Tanaka* [1999]. The existence of singular features in field line mapping is not surprising due to the fact that the field lines participating in reconnections pass through the diffusion region. As pointed out by *Cowley* [1973] and emphasized by *Crooker et al.* [1998] and *Tanaka* [1999], the field lines do not maintain their identities, and their motion does not match the plasma velocity throughout the reconnection process. When tracing the field lines from their solar wind ends, they are connected to different ionospheric ends at different times by changing partners. Although *Raeder et al.* [2000] did not discuss details on how this "entry window" is generated by the reconnection, their simulation provides a guide for looking for clues for understanding the driving mechanisms for the nightside cell. A detailed study of coupled magnetosphere-ionosphere convections using the global MHD simulation model of *Raeder* [1999] for this particular interval of 15 May 1997, is a topic of future study.

6. Summary

[37] The passage of the 14–16 May 1997 magnetic cloud produced a prolonged interval with large positive IMF B_y and northward B_z conditions ($B_y/B_z \gg 1$). It allows us to investigate driving mechanisms for the IMF B_y-related plasma convection and cusp field-aligned currents. The data presented in this paper include in situ observations of magnetic field, electric field, and electrons and ion fluxes from the FAST spacecraft at ~300–600 km altitude and global convection patterns from the AMIE procedure. Using the FAST single trajectory observations to validate the global convection patterns at key times and key locations, we have demonstrated that the AMIE procedure provides a reasonably good description of plasma circulations in the ionosphere.

[38] Despite different levels of convection, common features are found in the global morphology of the plasma convection during the interval of interest. When the IMF has a strongly positive B_y component under northward conditions, the direction of convection flow near the local noon is consistent with the antiparallel merging model. We find that a single clockwise convection cell develops in the dayside Northern Hemisphere, mainly circulating within the polar cap on open field lines. A second cell with counterclockwise convection is located in the nightside, circulating across the polar cap boundary. The observed two-cell convection pattern appears to be driven by the reconnection, as suggested by global MHD simulations when IMF $B_y/B_z \gg 1$ under northward IMF conditions. The magnetic tension force on the newly reconnected field lines drives the plasma to move from dusk to dawn in the polar cusp region near the polar cap boundary. The field-aligned currents in the cusp region flow downward into the ionosphere. The return field-aligned currents extend into the polar cap in the center of the convection cell. The field-aligned currents are found to close mainly through the Peterson currents in the ionosphere, which flow poleward from the polar cap boundary along the electric field direction.

[39] **Acknowledgments.** Guan Le thanks Carmen Liebrecht and Kristine Sigsbee for helping with FAST data analysis software. The WIND (R. P. Lepping, PI) and IMP-8 (A. Szabo, PI) key parameter data were provided by NSSDC CDDAW web. G. Lu was supported by NASA SEC Guest Investigator programs. R. J. Strangeway was supported by NASA.

[40] Hiroshi Matsumoto and Lou-Chuang Lee thank two reviewers for their assistance in evaluating this paper.

References

Block, L. P., and C.-G. Falthammar, The role of magnetic-field-aligned electric fields in auroral acceleration, *J. Geophys. Res.*, *95*, 5877, 1990.

Burch, J. L., et al., IMF By-dependent plasma flow and Birkeland currents in the dayside magnetosphere, 1, Dynamics Explorer observations, *J. Geophys. Res.*, *90*, 1577, 1985.

Burke, W. J., M. C. Kelley, R. C. Sagalyn, M. Smiddy, and S. T. Lai, Polar cap electric field structures with northward interplanetary magnetic field, *Geophys. Res. Lett.*, *6*, 21, 1979.

Burke, W. J., E. M. Basinska, N. C. Maynard, W. B. Hanson, J. A. Slavin, and J. D. Winningham, Polar cap potential distributions during periods of positive IMF by and bz, *J. Atmos. Sol. Terr. Phys.*, *56*, 209, 1994.

Carlson, C. W., R. F. Pfaff, and J. G. Watzin, The fast auroral snapshot (FAST) mission, *Geophys. Res. Lett.*, *25*, 2013, 1998.

Cowley, S. W. H., A qualitative study of the reconnection between the Earth's magnetic field and an interplanetary field of arbitrary orientation, *Radio Sci.*, *8*, 903, 1973.

Cowley, S. W. H., Magnetosphere-ionosphere interactions: A tutorial review, in *Magnetospheric Current Systems*, edited by S.-I. Ohtani et al., pp. 91, Geophys. Monogr. 118, AGU, Washington, D. C., 2000.

Crooker, N. U., Dayside merging and cusp geometry, *J. Geophys. Res.*, *84*, 951, 1979.

Crooker, N. U., Mapping the merging potential from the magnetopause to the ionosphere through the dayside cusp, *J. Geophys. Res.*, *93*, 7338, 1988.

Crooker, N. U., Reverse convection, *J. Geophys. Res.*, *97*, 19,363, 1992.

Crooker, N. U., and F. J. Rich, Lobe cell convection as a summer phenomenon, *J. Geophys. Res.*, *98*, 13,403, 1993.

Crooker, N. U., J. G. Lyon, and J. A. Fedder, MHD model merging with IMF By: Lobe cells, sunward polar cap convection, and overdraped lobes, *J. Geophys. Res.*, *103*, 9143, 1998.

Crowley, G., P. S. Cannon, C. G. Dozois, B. W. Reinisch, and J. Buchau, Polar cap convection for Bz northward, *Geophys. Res. Lett.*, *19*, 657, 1992.

Dungey, J. W., Interplanetary magnetic field and auroral zones, *Phys. Rev. Lett.*, *6*, 47, 1961.

Fedder, J. A., S. P. Slinker, and J. G. Lyon, A comparison of global numerical simulation results to data for the January 27–28, 1992, Geospace Environment Modeling challenge event, *J. Geophys. Res.*, *103*, 14,799, 1998.

Heelis, R. A., Interplanetary magnetic field effects on high latitudes ionospheric convection, in *The Polar Cusp*, edited by J. A. Holter and A. Egeland, p. 293–303, D. Reidel, Norwell, Mass. (imprint of Kluwer Acad.) 1985.

Heppner, J. P., and N. C. Maynard, Empirical high-latitude electric field models, *J. Geophys. Res.*, *92*, 4467, 1987.

Hill, T. W., Theoretical models of polar-cap convection under the inference of a northward interplanetary magnetic field, *J. Atmos. Sol. Terr. Phys.*, *56*, 185, 1994.

Huang, C.-S., D. A. Andre, G. J. Sofko, and A. V. Kustov, Super Dual Auroral Radar Network observations of ionospheric multicell convection during northward interplanetary magnetic field, *J. Geophys. Res.*, *105*, 7419, 2000.

Jordanova, V. K., C. J. Farrugia, R. M. Throne, G. V. Khazanov, G. D. Reeves, and M. F. Thomsen, Modeling ring current proton precipitation by electromagnetic ion cyclotron waves during the May 14–16, 1997, storm, *J. Geophys. Res.*, *106*, 7, 2001.

Knipp, D. J., A. D. Richmond, B. Emery, N. U. Crooker, O. de la Beaujardiere, D. S. Evans, and H. W. Kroehl, Ionospheric convection response to changing IMF direction, *Geophys. Res. Lett.*, *18*, 721, 1991.

Knipp, D. J., et al., Ionospheric convection response to a magnetic cloud: A case for 14 January 1988, *J. Geophys. Res.*, *98*, 19,273, 1993.

Lu, G., et al., Interhemispheric asymmetry of the high-latitude ionospheric convection pattern, *J. Geophys. Res.*, *99*, 6491, 1994.

Maezawa, K., Magnetospheric convection induced by positive and negative z component of the interplanetary magnetic field: Quantitative analysis using polar cap magnetic records, *J. Geophys. Res.*, *81*, 2289, 1976.

McCormac, F. G., T. L. Killeen, and J. P. Thayer, The influence of IMF By on the high-latitude thermospheric circulation during northward IMF, *J. Geophys. Res.*, *96*, 115, 1991.

Pfaff, R., et al., Initial FAST observations of acceleration processes in the cusp, *Geophys. Res. Lett.*, *25*, 2037, 1998.

Potemra, T. A., L. J. Zanetti, P. F. Bythrow, A. T. Y. Lui, and T. Iijima, By-dependent convection patterns during northward interplanetary field, *J. Geophys. Res.*, *89*, 9753, 1984.

Raeder, J., Modeling the magnetosphere for northward interplanetary magnetic field: Effects of electrical resistivity, *J. Geophys. Res.*, *104*, 17,357, 1999.

Raeder, J., O. Vaisberg, V. Smirnov, and L. Avanov, Reconnection driven lobe convection: Interball Tail Probe observations and global simulations, *J. Atmos. Sol. Terr. Phys.*, *62*, 833, 2000.

Reiff, P. H., Sunward convection in both polar caps, *J. Geophys. Res.*, *87*, 5976, 1982.

Reiff, P. H., and R. A. Heelis, Four cells or two? Are four convection cells really necessary?, *J. Geophys. Res.*, *99*, 3955, 1994.

Rich, F. J., and M. Hairston, Large-scale convection patterns observed by DMSP, *J. Geophys. Res.*, *99*, 3827, 1994.

Rich, F. J., D. A. Hardy, and R. H. Redus, Northward IMF and patterns of high-latitude precipitation and field-aligned currents—The February 1986 storm, *J. Geophys. Res.*, *95*, 7893, 1990.

Richmond, A. D., and K. Kamide, Mapping electrodynamic features of the high-latitude ionosphere from localized observations: Technique, *J. Geophys. Res.*, *93*, 5741, 1988.

Ruohoniemi, J. M., and R. A. Greenwald, Statistical patterns of high-latitude convection obtained from Goose Bay HF radar observations, *J. Geophys. Res.*, *101*, 21,743, 1996.

Russell, C. T., The configuration of the magentosphere, in *Critical Problems of Magnetospheric Physics*, edited by E. R. Dyer Jr., p. 1, National Academy of Sciences, Washington, D. C., 1972.

Saunders, M. A., Origin of the cusp Birkeland currents, *Geophys. Res. Lett.*, *16*, 151, 1989.

Smiddy, M., W. J. Burke, M. C. Kelly, N. A. Saflekos, M. S. Gussenhoven, D. A. Hardy, and F. J. Rich, Effects of high-latitude conductivity on observed convection electric fields and Birkeland currents, *J. Geophys. Res.*, *85*, 6811, 1980.

Sugiura, M., N. C. Maynard, W. H. Farthing, J. P. Heppner, B. G. Ledley, and L. J. Cahill Jr., Initial results on the correlation between the magnetic and electric fields observed from the DE-2 satellite in the field-aligned current regions, *Geophys. Res. Lett.*, *9*, 985, 1982.

Tanaka, T., Configuration of the magnetosphere-ionosphere convection system under northward IMF conditions with nonzero IMF By, *J. Geophys. Res.*, *104*, 14,683, 1999.

Troshichev, O. A., Global dynamics of the magnetosphere for northward IMF conditions, *J. Atmos. Sol. Terr. Phys.*, *52*, 1135, 1990.

Webb, D. F., R. P. Lepping, L. F. Urlaga, C. E. DeForest, D. E. Larson, S. F. Martin, S. P. Plunkett, and D. M. Rust, The origin and development of the May 1997 magnetic cloud, *J. Geophys. Res.*, *105*, 27,251, 2000.

Weimer, D. R., Models of high-latitude electric potentials derived with a least error fit of spherical harmonic coefficients, *J. Geophys. Res.*, *100*, 19,595, 1995.

G. Le and R. F. Pfaff Jr., Code 696, Laboratory for Extraterrestrial Physics, NASA Goddard Space Flight Center, Greenbelt, MD 20771, USA. (Guan.Le-1@nasa.gov)

G. Lu, High Altitude Observatory, NCAR, Boulder, Colorado, USA.

R. J. Strangeway, Institute of Geophysics and Planetary Physics, University of California, Los Angeles, California, USA.